Short Fiber–Elastomer Composites. Effects of Matrix and Fiber Level on Swelling and Mechanical and Dynamic Properties

LUIS IBARRA* and CELIA CHAMORRO

Instituto de Ciencia y Tecnología de Polímeros (C.S.I.C.), Juan de la Cierva 3, 28006 Madrid, Spain

SYNOPSIS

The effects of different types of elastomeric matrix (NR, SBR, CR, NBR) and several levels (10, 15, and 20 parts phr) of short fibers on mechanical properties of uncured and cured composites and on swelling behavior of composites in hydrocarbon solvent are studied. The variation of the dynamic properties, E', E'', and tan δ is determined as a function of deformation amplitude, temperature, and vibration frequency in composite materials subjected to dynamic deformation. The increase of fiber level does not limit the orientation ability of the fibers, which in all materials seemed to be above 70%. The addition of fiber markedly reduces maximum swelling and entails an increase in material stiffness. In addition, the amount of dissipated energy is increased and hence transformable into heat upon fiber incorporation, which can reach up to 16 times the value corresponding to the matrix alone, in addition to an increase with strain amplitude. The effect is most pronounced in the presumed direction of fiber orientation.

The marked reduction of elongation at break (up to values of 7–9% of those of unfilled samples) and the shape of stress–strain curves point to a good fiber–matrix adhesion. Dynamic glass transition temperature is displaced toward higher values as a consequence of matrix–fiber interaction, which increases proportionally to fiber level, thus proving a linear relationship between thermal displacement and the number of interactions between the two phases. By the same token, the apparent activation energy of the relaxation process is enhanced for fiber-containing materials as compared to the fiber-free matrix. The fiber composites present a less prominent yet broader transition zone.

INTRODUCTION

A previous work[1,2] on the influence of several fibers on mechanical and dynamic properties of composite materials, based on a filled SBR matrix, showed that polyester and polyamide short fibers are the most reinforcing fibers. A parallel study determined the influence of PET fiber level on the mechanodynamic behavior of materials based on natural rubber[3] and SBR,[4] both filled with sepiolite, a natural magnesium silicate. To promote the fiber to rubber adhesion, a RFS (resorcine–formaldehyde–silica) system was included in the compound recipes, and it was shown[5] that the substitution of sepiolite for silica gave positive results. Certain modifications of the curing system were also studied[6] to improve the efficiency of the adhesive system during vulcanization of composites based on SBR and polyester or polyamide short fibers.

Glass and carbon fibers, in spite of their good properties of adhesion to the matrix, are unsuitable for elastomer reinforcement because they are easily broken during mixing and so the final length–diameter ratio is markedly reduced. The importance of this parameter was studied[7] in composites with polyester and carbon fibers in EPDM matrices.

This study deals with the mechanical properties of uncured and cured compounds based on natural rubber (NR), styrene–butadiene rubber (SBR), polychloroprene rubber (CR), and nitrile rubber

* To whom correspondence should be addressed.

Journal of Applied Polymer Science, Vol. 43, 1805–1819 (1991)
 CCC 0021-8995/91/101805-15$04.00

(NBR), filled with 10, 15, and 20 parts by volume of polyester fiber per 100 parts by weight of polymer.

To get a deeper knowledge on the anisotropy and matrix–fiber interactions in these composites, measurements of maximum swelling in hydrocarbon solvents were carried out that would provide additional information on fiber orientation.

Because swelling depends also on matrix–fiber interaction, network densities of the different composites were determined.

The dynamic properties of composites can be measured at variable deformation amplitudes or at variable frequencies and temperatures, strain amplitude remaining constant in this case. This work reports on the results obtained with either experimental method. The first determines the zone of linear viscoelastic behavior, i.e., the area where the elastic component of the modulus, storage modulus, is independent of strain amplitude. The second type of measurement, at constant deformation within the linear response zone, supplies information about a highly relevant factor regarding the general properties of these materials: the interactions between the matrix and the fiber. Even if there is agreement in the relevant literature about the fibers to possess a unidirectional orientation, this fact was not confirmed in our case. This finding does not, however, invalidate the conclusions that may be reached.

The elastomeric matrix–fiber interactions cause immobility of the polymeric chains and, as a consequence, alterations are produced in certain material characteristics, such as glass transition temperature. The variable frequency tests yield the master curves, within the constrain by the application of the Williams-Laudel-Ferry (WLF) equations, which allow one to predict the viscoelastic behavior of these materials under conditions that cannot be produced by means of the presently available experimental methods.

EXPERIMENTAL

Materials

Sepiolite, a hydrated magnesium silicate of semireinforcing character, with the trade name Pansil (Tolsa S.A.), was used as additional filler in all compounds. Its specifications are as follows: screen residue, ASTM 325 mesh, none; particle size, more than 75% in the range 2–100 μm; specific gravity, 2; apparent density, 100–200 g/L; pH (10% aqueous suspension), 8; dibutyl phtalate adsorption, 200 $cm^3/100$ g (DBP number, 200); surface area (BET), 288 m^2/g.

Fibers were PET type, supplied by Velutex Flock S.A., with following characteristics: specific gravity, 1.38; length, 5–6 mm; diameter, 18 μm. They were used as delivered by the supplier, without any further treatment.

The RFS adhesive system was made up by 2.5 parts phr of Cohedur A, a formaldehyde donor from Bayer AG, and 2.5 parts phr resorcine. Instead of silica the filler Pansil was the third component.

Compound Preparation and Testing

All compounds were mixed under the same conditions, fibers being added at the end of the process and keeping always the same rolling direction to promote fiber orientation, as discussed in previous work. Compounds were finally sheeted, again in the rolling direction, into slabs of 2 mm thickness. Formulations are shown in Table I.

Curing characteristics were measured with a Monsanto Rheometer, at 150°C, 1°, and 1.67 Hz. All compounds were vulcanized at their respective t'_c (90).

Green strength was measured with rectangular test pieces of 25 × 150 × 2 mm, shaped by heating at 120°C for 2 min under slight pressure. The test pieces were then conditioned for 3 h at standard temperature and tested in a Instron machine, model 1026, at an elongation rate 500% min^{-1}.

Shore A hardness was determined according to ISO 7619, tensile properties according to ISO 37, and tear strength according to ISO 816 (Delft test piece).

Swelling Measurements

For the swelling test, rectangular test pieces, 25 mm long, 10 mm wide, and 2 mm thick were used. The test pieces were cut with its long axis parallel to the grain (see Fig. 1). Length, width, and thickness were accurately measured before and after 48-h immersion at 30°C in *n*-heptane for NR and SBR matrices and in toluene for CR and NBR based materials.

Dynamic Properties

The dynamic properties were measured on a Metravib viscoanalyzer, which, based on the principle of nonresonant forced vibrations, allows one to work at a frequency range from 5 to 1000 Hz, temperatures between −120 and 300°C, and a deformation amplitude of up to 500 μm, irrespective of whether it is associated or not to static predeformation.

In the variable strain tests, variation ranged over

Table I Formulation of Composites

	NR[a]	SBR[b]	CR[c]	NBR[d]
Polymer	100	100	100	100
OZn	5	5	5	5
OMg	—	—	4	—
Stearic acid	2	2	1.25	1.25
Sepiolite[e]	35	35	35	35
Triethanolamine	1.75	1.75	1.75	1.75
Naphtenic oil	—	—	10	—
Dibutyl phtalate	—	—	—	10
2-Mercaptoimidazoline[f]	—	—	0.5	—
MBTS	—	—	—	2
DOTG	0.3	0.3	—	0.8
CBS	0.8	0.8	—	—
Sulfur	2	2.2	—	2
Formaldehyde donor[g]	2.5	2.5	2.5	2.5
Resorcine	2.5	2.5	2.5	2.5
Fiber[h]		Variable		

[a] SMR 5 CV.
[b] SBR 1502.
[c] Neoprene WRT.
[d] Polysar Krynac 805.
[e] Pansil, from Tolsa SA.
[f] NA-22, from DuPont.
[g] Cohedur A, Bayer AG.
[h] 13.8: 20.7 and 27.6 parts by weight (equivalent to 10, 15, and 20 parts by volume).

1–400 μm at a temperature of 25°C and a frequency of 11 Hz.

The tests with temperature and frequency variables comprised a temperature range of −80 to 60°C, and the experimental vibration frequencies were 7.8, 15.6, 31.2, and 62.5 Hz. Deformation amplitude in all cases was held within the linear response zone.

In both series a parallelepipedic sample dimensioned 16 × 4 × 16 mm was subjected to a compression–tension test. The shape of the sample allowed one to work with stresses applied longitudinally (L) and transversally (T) to the preferential fiber orientation.

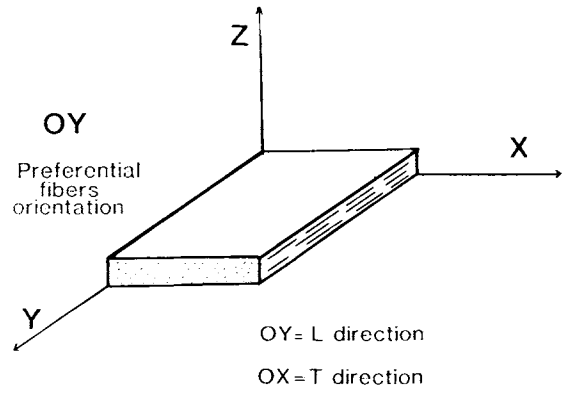

Figure 1 Schematic diagram of a composite structure.

Adjustment of the experimental sites and peak determination were done with the aid of a microprocessor program with polynomial adjustment of degree n.

RESULTS AND DISCUSSION

Uncured Properties

Vulcanization

Table II shows the vulcanization parameters of the different composites. For any matrix type fiber addition causes an increase of minimum and maximum torque, M_L and M_H, and sometimes of torque increments. The use of an RFS adhesive system increases curing times, specially with the more polar matrices CR and NBR. Scorch times are not influenced either by fiber or adhesive addition.

Green Strength

Figure 2 shows the relative green strength versus fiber level for each matrix; relative green strength is defined as the ratio between the composites green

Table II Vulcanization Parameters

Polymer	Fiber	M_H	M_L	M	t'_c (90)	t'_{s2}
NR	0	36.6	3.4	33.2	6.5	2.5
	10	41.6	4.4	37.2	8.5	3.0
	15	47	4.6	43.6	11.2	3.2
	20	47.8	4	43.8	10.5	3.2
SBR	0	47	6.8	40.2	58	4
	10	49	9.5	39.5	67	3.75
	15	57	11	46	78	3.75
	20	50	10	40	75	4.25
CR	0	41	7.5	33.5	44	2.75
	10	54	10.4	43.6	70	1.75
	15	61	14	47	80	1.75
	20	50	12.5	37.5	85	1.3
NBR	0	45.5	5.5	40	15	2.5
	10	48	8	40	31	2.25
	15	56	7.5	48.5	33	1.75
	20	67	10	57	41	2

strength and that of the unfilled matrix. Figure 2(a) shows the values measured in a parallel direction with respect to sheeting direction, and Figure 2(b) shows those measured in a perpendicular direction to the latter. With all matrices the marked anisotropy of the composites is evident, presumably due to fiber orientation in the milling direction.

In the direction of the presumed orientation, green strength increases with fiber level, although in the case of the NR matrix it seems to level off above 15 parts phr. In the direction perpendicular to orientation no significant difference is observed, except a slight increase in the case of NR.

According to Foldi,[8] these green strength values

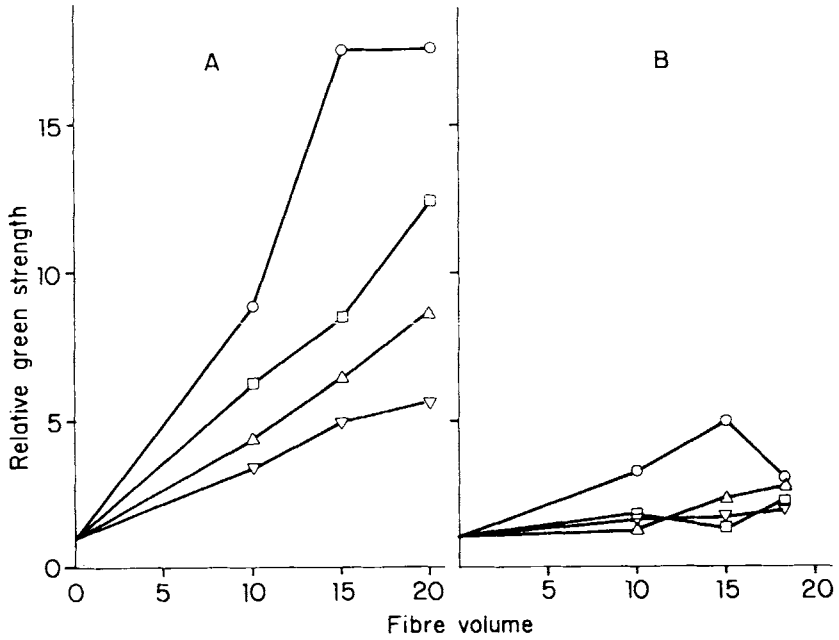

Figure 2 Relative green strength versus fiber content: (⊙) natural rubber; (▽) SBR; (△) CR; (⊡) NBR. (a) Along orientation direction; (b) across orientation direction.

Table III Fiber Orientation (%) Estimated from Green Strength Measurements

Fiber Volume	NR	SBR	CR	NBR
10	73.2	62.8	77.5	78.4
15	77.8	74.4	73.2	86.9
20	85.2	74.5	76.3	84.7
Average (%)	78.7	72.2	75.7	83.3

can be used for a quantitative estimation of fiber orientation. Table III summarizes the estimated percentage orientation, calculated by the formula

$$\frac{R_L/R_{L,0}}{(R_L/R_{L,0}) + (R_T/R_{T,0})}$$

where, R_L and R_T mean green strength values when the main axis of the test pieces runs longitudinally or transversally with respect to sheeting direction, respectively, and the suffix 0 refers to the corresponding values of the unfilled matrix. Higher levels of fiber do not hinder fiber orientation. Orientation seems to be maximum with the NBR matrix and minimum in SBR composites.

Mechanical Properties

The test results are shown in Table IV.

Shore A Hardness

As expected, the fibers increase markedly the composite hardness; there is a continuous increase of hardness with increasing fiber level.

Tensile Strength

The results depend on matrix type. With amorphous matrices, SBR and NBR, there is a gradual increase of tensile strength with fiber level, more marked when tested parallel to fiber orientation. With CR and NR matrices, when tested parallel to fiber orientation, tensile strength drops initially to rise again with fiber level 15 parts phr or higher; when tested

Table IV Mechanical Properties

	Along Orientation				Across Orientation			
Fiber	NR	SBR	CR	NBR	NR	SBR	CR	NBR
				(a) Shore A hardness				
0	61.6	61.3	66.8	67.2	—	—	—	—
10	80.9	82.3	84.3	85	—	—	—	—
15	86.4	86.1	85.1	86	—	—	—	—
20	88.2	89.8	86.6	89.1	—	—	—	—
				(b) Tensile Strength, MPa				
0	14.4	5.7	11.5	8.9	14.6	6	12	8.7
10	9.4	6.2	10.8	10.5	8.9	6.6	8.9	9.6
15	10.2	7.5	10.5	11.1	8.8	7.1	7.1	9.2
20	13.2	8.4	13.6	15.1	8.3	6.6	6.6	10.6
				(c) Tear Strength, N				
0	43.4	31.1	64.3	38	43.4	31.1	31.4	38
10	66.2	53.9	86.8	80	46.7	49.7	49.6	72.2
15	99.3	69.9	94.3	107.7	54.2	48.6	61.5	69.2
20	127.2	100.6	118.3	130.2	60.4	58.5	77.7	78.1
				(d) Elongation at Break, %				
0	404	260	351	315	402	254	245	311
10	254	235	156	164	260	332	195	272
15	100	48.5	51	74.5	224	222	144.5	186
20	36.2	24.2	24.2	30.5	212	111	191	115.5

at right angle with fiber orientation, tensile strength falls continuously with fiber level. These results may be attributed to some hindrance of crystallization of the matrix on tensile strain.

Tear Strength

In every condition a substantial increase of tear strength is observed, probably because fibers make more difficult the crack propagation. Again the anisotropic effect is clearly noticeable. Reinforcement is most marked with the NBR matrix.

Elongation at Break

There is a continuous drop of elongation at break that is proportional to fiber level. The reduction is more marked when the test is carried out in the direction of fiber orientation.

Tensile Stress–Strain Characteristic

Besides the effects on ultimate properties, the addition of fiber gives rise to a marked increase of stiffness. Figure 3 shows the tensile stress–strain curves of composites, tested with test pieces cut parallel to fiber orientation.

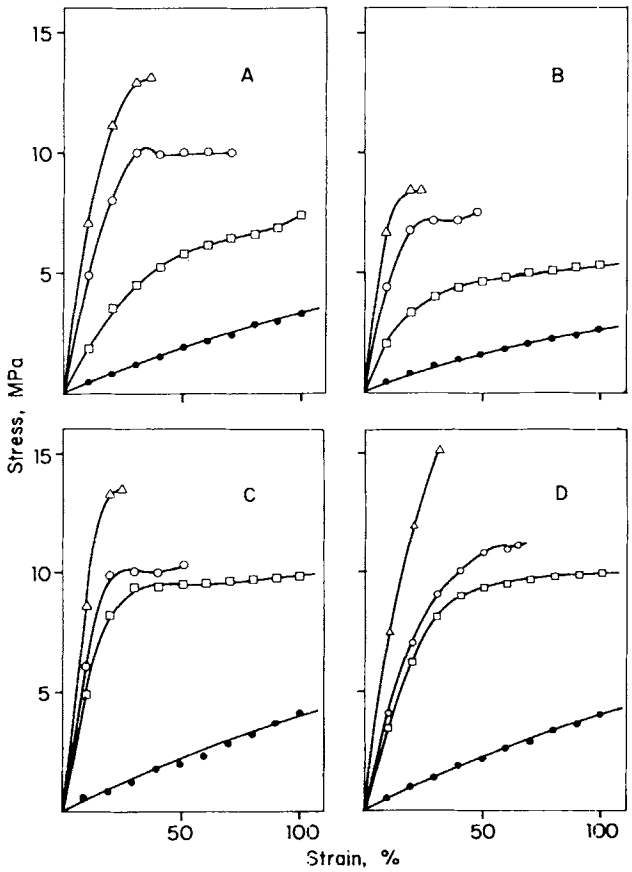

Figure 3 Stress–strain curves of composites: (a) NR; (b) SBR; (c) CR; (d) NBR. (●) without fibers; (□) 10 parts v/w of fibers; (⊙) 15 parts of fibers; (△) 20 parts of fibers.

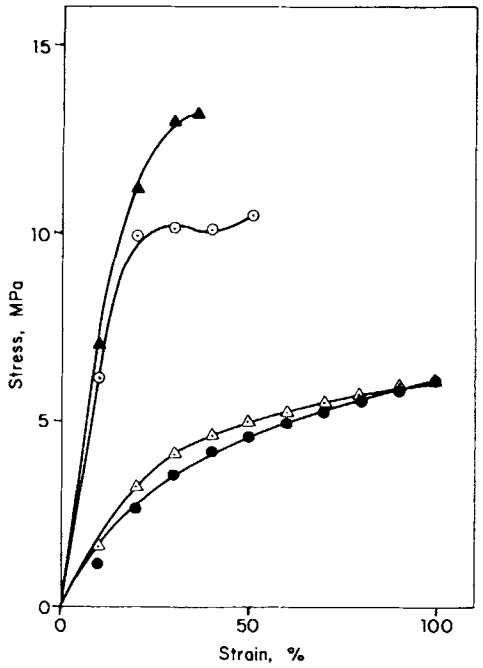

Figure 4 Stress–strain curves. (▲) NR/20 volumes PET composites, along orientation direction; (△) NR/20 volumes PET composite, across orientation direction; (⊙) CR/15 volumes PET composite, along orientation direction; (●) CR/15 volumes PET composite, across orientation direction.

Although there are differences among the several matrix types, all curves follow a similar pattern. Initially a very rapid stress growth takes place, even with low fiber level; this may reflect the existence of strong matrix–fiber bonds that restrict the deformation ability of the composite.

From ca. 30% elongation there is a tendency for the stress to level off, probably associated with the separation of fibers from the matrix, eventually leading to the failure of the polymeric matrix.

Once more a marked anisotropy is clearly observed in these properties, as shown in Figure 4, where, by way of example the tensile stress–strain curves of two materials with test pieces cut along and across the direction of fiber orientation are represented. These latter come close to the curves of unfilled matrices shown in Figure 3.

Swelling

According to Coran et al.,[9] the linear swelling ratio, i.e., the ratio of original dimension to swelled di-

mension in any direction forming an angle θ to fiber orientation, a_θ, is given by expression (1):

$$a_\theta^2 = (a_T^2 - a_L^2)\sin^2\theta + a_L^2 \quad (1)$$

where a_T and a_L stand for the swelling ratios transversal and longitudinal, respectively. To test its validity and the rightness of the assumption of fiber orientation in the grain direction, measurements of linear swelling ratios at different θ values were carried out.

It is stating the obvious to say that for each composite family network density would be determined by the curing system. If there was no rubber–fiber interaction, the same density values could be expected for the whole family, irrespective of fiber level. If there exists, however, strong interfacial adhesion, the rubber–fiber bonds would be computed as interchain bonds and crosslink density would be increased.

Crosslink densities were determined by the Flory–Rhener equation[10]:

$$\nu_e = \frac{-|\ln(1 - v_r) + v_r + \mu v_r^2|}{V_1(v_r^{1/3} - v_r/2)}$$

where ν_e stands for crosslink density or actual network density in mols, v_r is the swollen rubber volume fraction, V_1 is the molar solvent volume, and μ stands for the Huggins parameter of polymer–solvent interaction.

v_r was determined either from linear deformation[9] or from the swollen and dry weights of the samples, following expressions (2) and (3), respectively;

$$v_r = 1 - \frac{v_{nn}}{a_L a_T a_Z} - v_{nn} \quad (2)$$

$$v_r = \frac{(1 - v_{nn})}{(M_s/M_0 - 1)\,\sigma_{sol}/\sigma_{comp}} + (1 - v_{nn}) \quad (3)$$

where v_{nn} is the fraction in volume of material components unaffected by the solvent (zinc oxide, filler, fiber, etc.), M_0 and M_s are the composite weight before and after swelling, σ_{sol} and σ_{comp} are solvent and density composite, respectively.

Table V shows the average values for v_r resulting from both methods, crosslink densities and crosslink density increments, over that of the matrix. In general, crosslinking density increases proportionally to fiber level. The larger density increments are observed with SBR composites and the smallest ones with NBR composites. These differences are attributed to a larger number of rubber–fiber bonds in the former, probably due to a greater efficiency of the rubber to fiber adhesion system induced by the matrix.

Table VI shows the linear swelling ratios for all composites. In the direction of the presumed fiber orientation, a_L, with composites based on SBR and CR swelling is practically inhibited even with the lowest fiber concentration, with NR composites is

Table V v_r Values and Crosslinking Densities[a]

Matrix	Fiber Volume	v_r	$\nu \times 10^4$	$\Delta\nu$
NR	0	0.3231	2.85	—
	10	0.3456	3.45	0.60
	15	0.3660	4.06	1.21
	20	0.3975	5.18	2.33
SBR	0	0.3712	2.79	—
	10	0.4041	3.74	0.96
	15	0.4432	5.19	2.41
	20	0.4526	5.61	2.86
CR	0	0.2376	2.70	—
	10	0.2717	3.70	1.00
	15	0.2908	4.35	1.65
	20	0.2745	3.79	1.09
NBR	0	0.3286	4.40	—
	10	0.3344	4.62	0.22
	15	0.3411	4.87	0.47
	20	0.3491	5.21	0.81

[a] v_r is the mean value obtained from eqs. (2) and (3). μ values employed in v_r determinations: system NR/*n*-heptane, 0.433; SBR/*n*-heptane, 0.515; CR/toluene, 0.342; NBR/toluene, 0.419; according Shvarts.[11]

Table VI Swelling of Composites

Matrix	Fiber Volume	a_L	a_T	a_z	Percent Change in Volume[a]	Percent Restriction of Swelling[b]
NR	0	1.32	1.23	1.66	270	—
	10	1.17	1.27	1.74	259	11.3
	15	1.00	1.16	1.89	219	26.3
	20	1.00	1.16	1.77	205	33.0
SBR	0	1.27	1.27	1.50	242	—
	10	1.03	1.23	1.65	209	20.5
	15	1.00	1.11	1.71	190	29.9
	20	1.00	1.10	1.67	184	33.1
CR	0	1.31	1.35	1.90	259	—
	10	1.02	1.18	2.00	241	13.6
	15	1.00	1.17	2.00	234	18.5
	20	1.00	1.19	2.01	239	19.3
NBR	0	1.31	1.30	1.52	259	—
	10	1.11	1.29	1.67	239	14.6
	15	1.08	1.26	1.67	227	21.2
	20	1.07	1.21	1.70	220	25.4

[a] Calculated from linear dimensional changes.
[b] Calculated with respect to volume that would be expected from the swelling of the matrix fraction in the composite.

necessary to reach the 15 parts phr fiber to get that result, whereas with NBR composites, although a considerable swelling constraint is observed, in all instances some swelling remains. This is just the opposite of what could be expected from the extent of fiber orientation estimated from green strength measurement, which ranked the composites in the following decreasing order:

$$\text{NBR} > \text{NR} > \text{CR} > \text{SBR}$$

This discrepancy can be explained assuming that, besides fiber orientation, matrix–fiber adhesion has a very pronounced influence on swelling. The increase of network density due to the presence of fibers is maximum in SBR composites and minimum in NBR composites.

The inequality between the values a_T and a_Z means that the orientation of the fibers is not perfectly unidirectional. The swelling along Z axis, what in accordance with other authors can be interpreted as due to the flow produced during molding, could tend to slightly disturb the fibers on the XY plane, while at the same time would favor fiber orientation in direction Y on the YZ plane.

Overall, volumetric swelling decreases with increasing fiber level, with the final figures lower than what would be expected from the swelling of the sole matrix fraction of composites, as shown in the last column of Table VI.

Figure 5 shows dimensional swelling variation with the angle θ between measurement direction and preferential fiber orientation. In all cases swelling increases with θ, which confirms a preferential fiber orientation in the grain direction (Y axis). Fitting of experimental points with the straight lines according Eq. (1) is reasonably good. According to Noguchi et al.,[12] the steeper the line, the higher the degree of fiber alignment. This technique confirms the previous results that fiber orientation is highest in NBR composites and lowest in SBR.

Dynamic Properties

Properties at Variable Strain Amplitude

1. *Storage Modulus, E'.* Fiber addition reduces the linear response zone of the modulus vis à vis deformation for certain samples to a very narrow span. This linear zone is likewise diminished as a consequence of the amount of fiber added to the composite.

For deformations between 0.01 and 2% (maximum strain to be achieved under the experimental conditions), a progressive decrease of the modulus takes place that is attributable to fiber–matrix bond

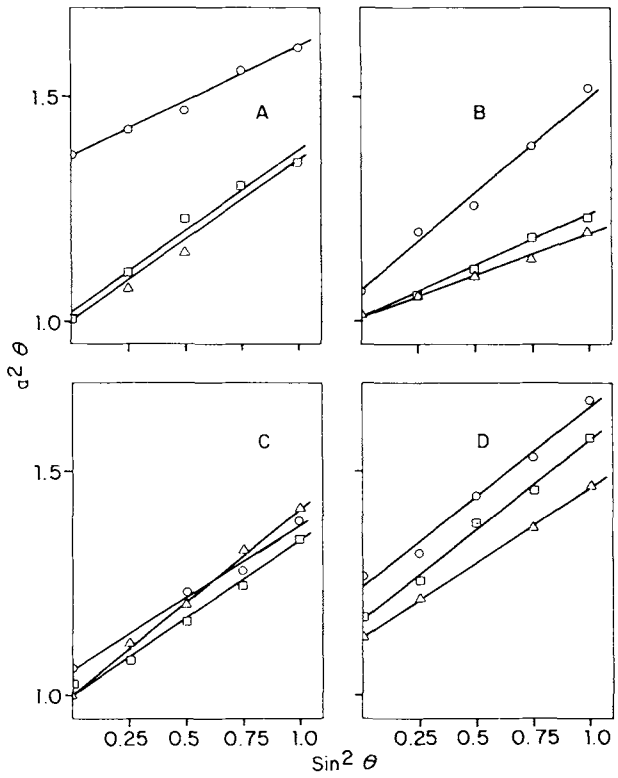

Figure 5 Swelling variation with angle θ according to expression (1): (a) NR matrix; (b) SBR matrix; (c) CR matrix; (d) NBR matrix. The points on the straight lines represent experimental points: (⊙) 10 PET volumes; (⊡) 15 PET volumes; (△) 20 PET volumes.

ruptures, which increment proportionally to the magnitude of the imposed strain.

Table VII shows the modulus E' values for low deformation ranges (0.002%, E'_0, as well as those for 2% deformation, which come close to the E'_∞ value, together with $\Delta E'$ values obtained as the differential, which together represent the total energy storage potential.[13]

Figure 6 represents $\Delta E'$ variation plotted against crosslinking density ($\Delta\nu$), as one of the ways to account for effective matrix–fiber bonds. There exists a direct relationship between both parameters in such a way that, the number of interfacial bonds being equal, the steeper slope is indicative of greater interfacial interaction implying a lesser modulus drop.

On the other hand, these composites present anisotropy with regard to fiber orientation. Figure 7 shows modulus E' variation as a function of deformation for composites CR-10 and CR-15, taking into account the direction of stress application, longitudinal (L) or transversal (T) with respect to preferential fiber orientation.

When deformations are applied transversally, the value of the modulus is lower for any fiber level than the corresponding values obtained from longitudinal measurements, yet both are higher than the values for the fiber-free matrix. The linear response zone is wider, although it does not reach the extension of that of the matrix.

Table VII Storage Modulus, E', Values at Very Low and Medium Deformation Ranges

Reference Number	Sample	E'_0 (MPa)	E'_2 (MPa)	ΔE (MPa)
1	NR-0	15.2	9.5	5.7
2	NR-10	121	50	71
3	NR-15	202	65	137
13	NR-20	159	55.7	103.3
4	SBR-0	9.9	7.9	2.0
5	SBR-10	109	58.5	50.5
6	SBR-15	162	62	100
14	SBR-20	185	55	130
7	CR-0	13.0	9.4	3.6
8	CR-10	144	45	99
9	CR-15	219	53.2	165.8
15	CR-20	159	55.7	103.3
10	NBR-0	10.2	8.6	1.6
11	NBR-10	102	57.5	44.5
12	NBR-15	143	84	59
16	NBR-20	197	73.1	113.9

[a] E'_2 represents the storage modulus at 2% deformation.

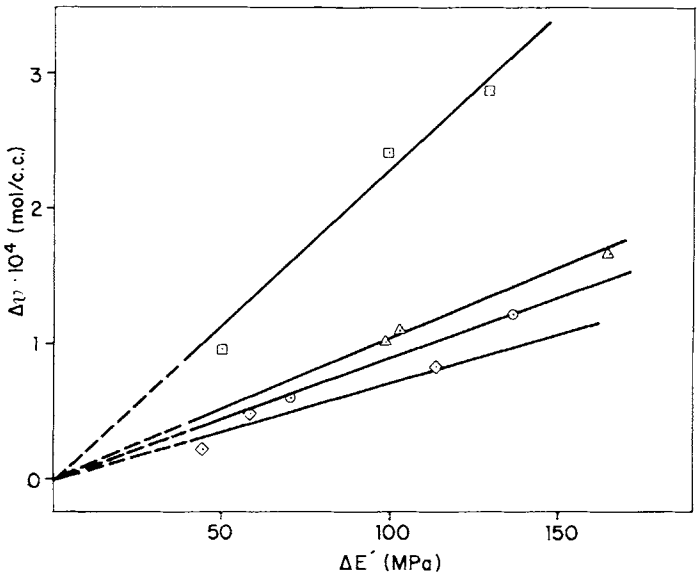

Figure 6 Ratio between network density ($\Delta\nu$) and total energy storage potential ($\Delta E'$). (⊙) NR matrices; (⊡) SBR matrices; (△) CR matrices; (◇) NBR matrices.

2. *Loss Modulus, E″.* Fiber incorporation enhances the loss modulus building up a peak, which is the higher fiber level. The behavior of these materials with regard to E'' is similar to that observed by Payne[14] in carbon black samples. The peak is located in the zone where E' variation is the fastest. Peak intensity is related to fiber content.

The effect of directional application of strain is shown in Figure 8 for SBR composites. In transversal application the peak is less pronounced and shows the same deformation value as the fiber-free matrix. Peak displacement toward lower deforma-

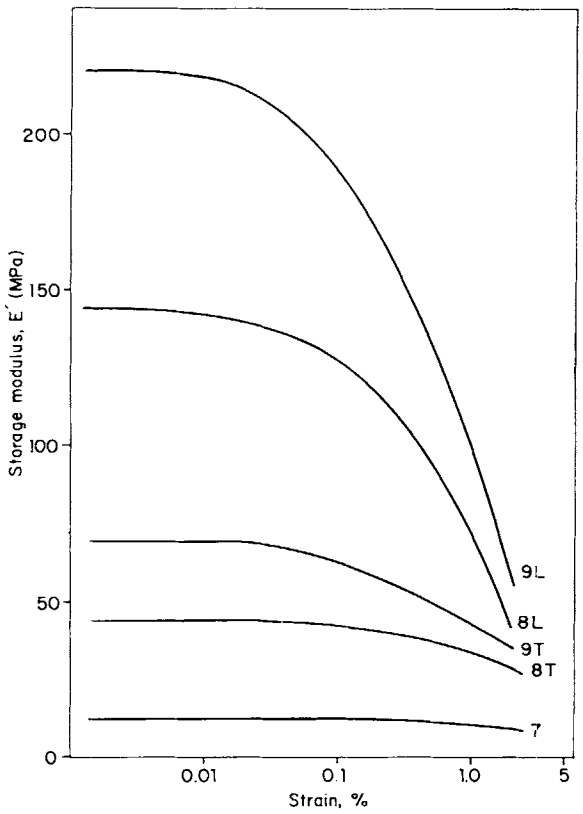

Figure 7 Effects of directional strain application on modulus E' variation. CR based on composites: (L) longitudinal; (T) transversal.

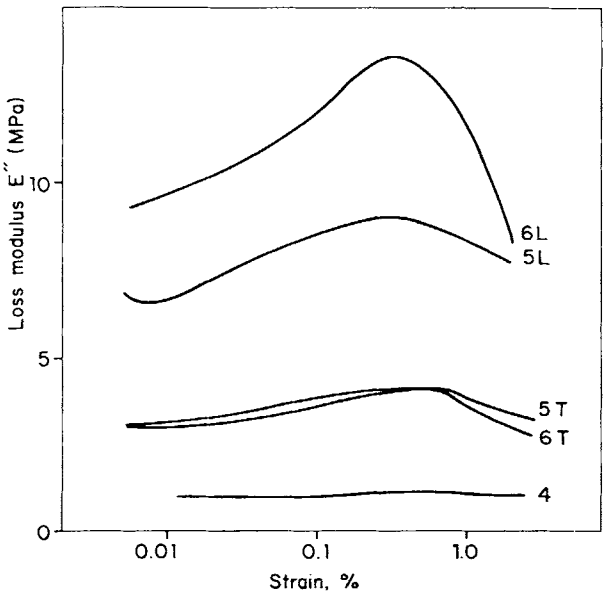

Figure 8 Effects of directional deformation application on E'' variation. SBR based on composites: (L) longitudinal; (T) transversal.

Table VIII Dissipated Energy (J/m³ sg) × 10^{-4} of Composite Materials as a Function of Strain Applied Longitudinally (*L*) and Transversally (*T*)

	L		*T*	
Sample	0.01%	0.1%	0.01%	0.1%
NR-0	0.31	0.34	0.31	0.34
NR-10	2.02	3.0	1.27	1.9
NR-15	3.04	4.7	1.37	2.04
NR-20	3.5	5.5	1.55	2.34
SBR-0	0.32	0.34	0.32	0.34
SBR-10	2.3	2.9	1.05	1.27
SBR-15	3.3	4.35	1.09	1.32
SBR-20	4.8	5.18	1.95	2.6
CR-0	0.37	0.40	0.37	0.40
CR-10	3.45	4.08	1.24	1.4
CR-15	4.87	6.4	1.81	2.2
CR-20	4.04	4.8	1.55	1.6
NBR-0	0.45	0.45	0.45	0.45
NBR-10	3.27	3.62	1.53	1.7
NBR-15	3.68	4.19	1.59	1.74
NBR-20	5.49	6.63	2.7	3.25

tion ranges is related to the degree of matrix–fiber interaction.

The enhanced loss modulus values evidence the fact that fiber-reinforced materials possess a higher dissipation energy, whenever this energy, which is converted into heat, is related to the E'' value, which actually is accountable for the greater heat generation. In Table VIII the dissipation energies of the different composites are expressed for two deformation amplitudes and in both the *L* and *T* directions. The presence of fiber causes an increase in heat build-up, as compared to the unreinforced material, which can be 6–16 times that of the matrix if the strain is applied in the direction of fiber orientation and 3–8 times when applied transversally, depending on fiber volume.

Properties at Variable Temperature

Variation of the storage modulus E' with temperature is represented in Figure 9 for different materials. The highest moduli appear in the low-temperature range near glass transition of the matrix, and increase proportionally to fiber level.

On increasing the temperature, the modulus diminishes until it stabilizes, coinciding with the elastic zone of the material. This transition zone between the glass and the elastic state is less prominent for fiber composites, and hence the modulus drop is smaller. As a consequence, such composites are less sensitive toward temperature variation.

Variation of the loss factor tan δ with temperature shows a peak, that at low frequencies corresponds to the dynamic glass transition temperature of the elastomeric matrix, where the damping effect is greatest. For short fiber composites the relaxation

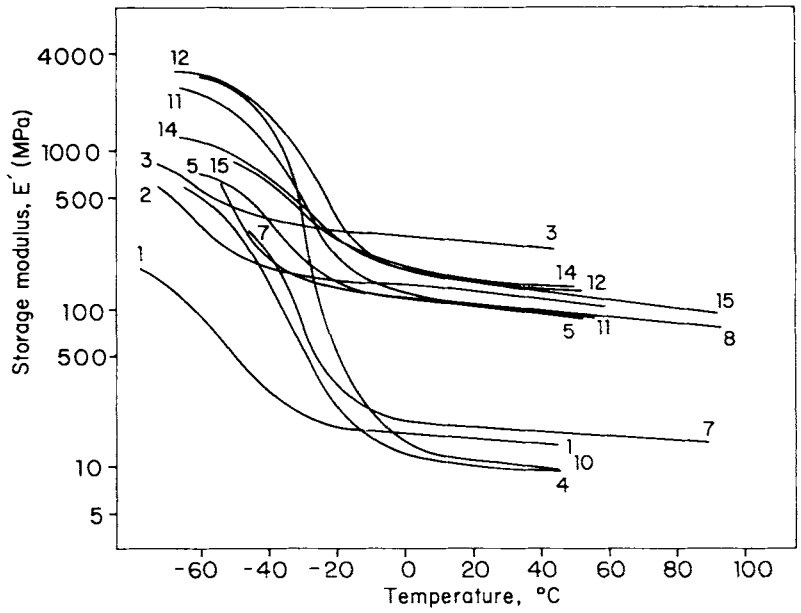

Figure 9 Storage modulus, E', as a function of temperature. Frequency 7.8 Hz. Longitudinal applied strain. The numbers above the curves correspond to those indicated in Table VII.

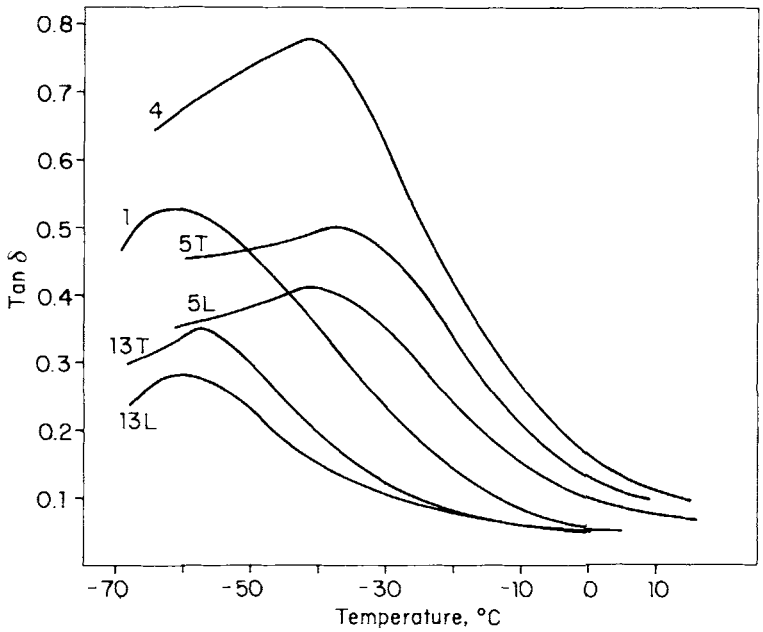

Figure 10 Variation of the loss factor tan δ with temperature. Conditions as in Figure 9: (L) longitudinal; (T) transversal measurements.

spectrum is similar to that of the matrix, presenting a single peak corresponding to matrix glass transition in the experimental temperature range.

Figure 10 shows tan δ variation with temperature for the composites NR-0, NR-20, SBR-0, and SBR-20 in longitudinal (L) and transversal (T) measurements. Damping depends on fiber level and orientation. The T values are intermediate between those of the matrix and the L measurements. The peaks are observed to shift toward higher temperatures due to the immobilizing effect of the fibers on the polymeric chains, a phenomenon which is more strongly differentiated in transversal measurements. Figure 11 indicates the ratio between the temperature increment T and the fiber–matrix bonds $\Delta\nu$ measured in terms of crosslinking density.

Properties at Variable Frequency

The dynamic properties depend on vibration frequency in the sense that the E' and E'' moduli increase proportional to frequency, as well as the damping factor tan δ. When dynamic strain is applied longitudinal to the direction of the fibers, these latter can contribute more strongly, hence lessening the damping effect. It has been proven[15] that, when measuring tan δ as a function of temperature, matrix and fiber relaxation can be demonstrated more accurately in transversal applications. This is why the relaxation zone was studied in composites to which strain had been applied transversal to fiber orientation.

From this peak displacement it is possible to determine an apparent activation energy of the relaxation process, assuming a linear equation, as expressed in (4):

$$\log f = \log f_o + \Delta H/2.303R*T \qquad (4)$$

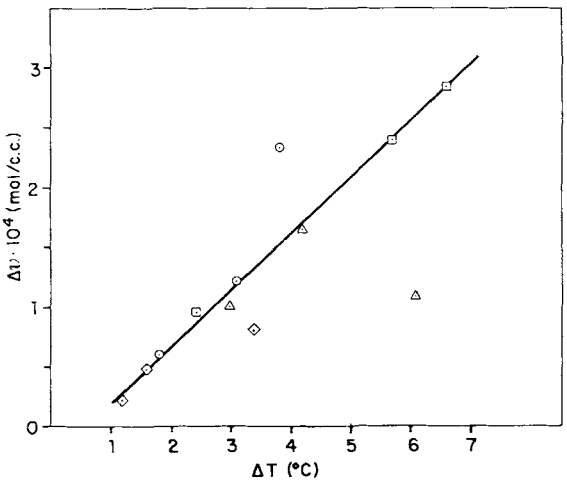

Figure 11 Correlation between damping peak shifts (ΔT) and matrix–fiber bonds ($\Delta\nu$). Frequency 7.8 Hz (⊙) NR matrices; (⊡) SBR matrices; (△) CR matrices; (◇) NBR matrices.

where ΔH is the apparent activation energy and T stands for the temperature of the peak at frequency f; R is the gas constant, at absolute temperature.

Table IX shows the peak temperatures as a function of frequency, as well as the computed activation energy values. At any frequency, temperature increases proportionally to fiber level. For the same material the temperature moves toward a higher value upon incrementing vibration frequency. By the same token, upon increasing the fiber portion, activation energy also grows. These higher energy values are associated with the existence of interactions deriving from matrix–fiber bonds.[16]

Fiber addition, in general terms, gives rise to a reduction of the damping effect, which on the whole increases with the frequency.

Master Curves

The measurements conducted at different temperatures and frequencies allowed for the application of the reduced variable method to storage modulus E',[17] which, in turn, makes it possible to establish the master curves of the different materials (Fig. 12) after calculating the value of the horizontal displacement α_T.

Generally, all curves present two characteristic zones: the "plateau" and the transition zones, although NBR-based materials show, in addition, a glass zone at high frequencies or low temperatures.

For all materials the zone intersection frequency W_{tr}[18] diminishes for fiber-reinforced composites, the higher the fiber content, which, among other things, confirms a broadening of the transition zone. The modulus values are congruent for all composites of identical matrix in the high-frequency range, which is indicative of the fact that in this range or at very low temperatures material properties are exclusively matrix-dependent.

CONCLUSIONS

With the four matrix types studied, fiber level seems to have no marked effect on the orientation ability.

Green strength of composites increases substantially when measured in the sense of the fiber orientation and does not vary significantly when tested across that direction. The strength increases with fiber level, but with the matrix based on NR, it levels off at 15 parts phr fiber.

An improvement of tear strength is observed with all matrix types and fiber levels. The increase is particularly noticeable when tested in such a way that tear propagation direction runs across the orientation sense.

When tested in tension in the same direction of the oriented fibers, these cause a marked increase of the composite stiffness up to ca. 30% elongation,

Table IX Maximum Damping Temperatures as a Function of Frequency and Activation Energies of the Relaxation Process

Sample	7.8	15.6	31.2	62.5	ΔH (kJ/mol)
NR-0	−60.9	−58.5	−56	−53.6	110.2
NR-10	−59.1	−57.3	−55.5	−53.7	150.3
NR-15	−57.8	−55.4	−54.3	−52.4	154.9
NR-20	−57.1	−55.6	−54.2	−52.3	175.5
SBR-0	−40.3	−37.1	−33.9	−30.6	99.9
SBR-10	−37.9	−36.9	−34.9	−31.5	146.3
SBR-15	−34.6	−32.7	−31.1	−28.4	164.6
SBR-20	−33.7	−32.1	−31.3	−28.9	216.3
CR-0	−41	−37.4	−35.9	−34.9	141.7
CR-10	−38	−35.7	−33.4	−31.0	140.1
CR-15	−36.8	−35.2	−33.6	−32.5	226
CR-20	−34.9	−33.6	−32.3	−30.5	228.1
NBR-0	−23.4	−21.5	−18.6	−14.8	127.8
NBR-10	−22.2	−20.3	−18.3	−16.4	188.6
NBR-15	−21.8	−20.3	−18.4	−15.5	215.5
NBR-20	−20	−17	−15.4	−13.7	227.9

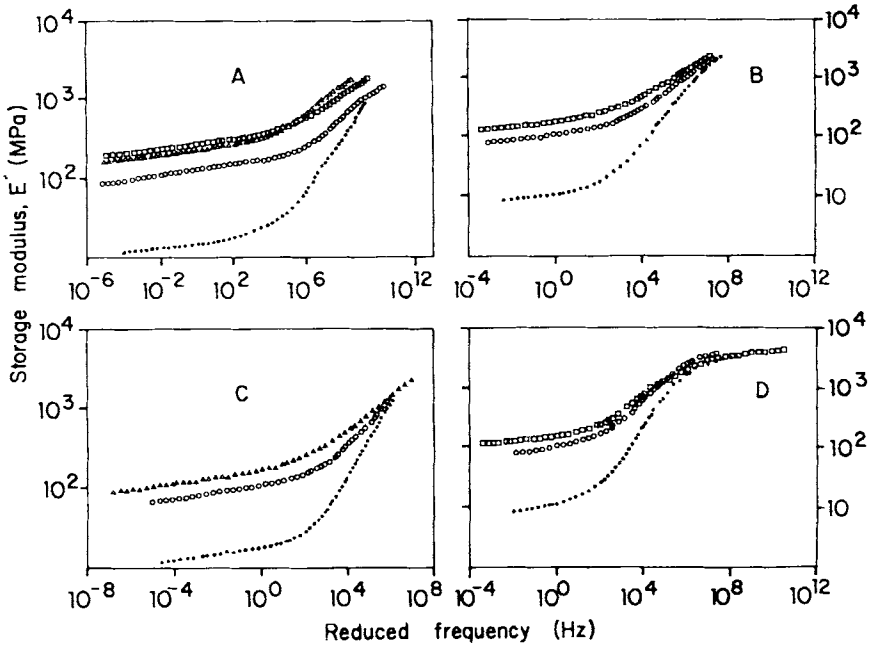

Figure 12 Composite master curves. (●) Polymeric matrices; (⊙) matrices with 10% fiber volume; (□) with 15% fiber volume; (△) with 20% fiber volume. (A) NR; (B) SBR; (C) CR; (D) NBR. In all cases the reference temperature is 0°C.

reflecting a strong matrix–fiber adhesion. At higher elongation, stress–strain curves level off, probably due to breakage of matrix–fiber bonds.

Short fibers markedly reduce swelling of composites in hydrocarbon solvents. The effect is most pronounced in the presumed direction of fiber orientation. Matrix nature influences the extent of the fiber effect, which is maximum with SBR composites followed by CR composites and minimum with composites based on NBR.

These findings are paralleled by relative increases in crosslinking densities attributed to larger number of rubber–fiber bonds. Presumably both characteristics, fiber orientation and rubber–fiber interaction, influence swelling extent, but the effect of the latter seems to exceed that of the former.

For high deformations, measured in our case up to 2%, the E' values are influenced by the fiber level and by the matrix–fiber bonds in such a way that there exists a direct correlation between modulus decrease and crosslinking density of the composites.

Fiber-containing materials are less temperature sensitive and present a transition zone between glass and elastic behavior that is less prominent yet wider and is detectable in the respective master curves. This effect increases as a function of the fiber level.

Fiber composites present a higher loss modulus E'', which means that heat generation is greater in these materials, as a function of fiber level and strain amplitude.

Matrix–fiber interaction translates into enhanced apparent activation energy of the relaxation process, as well as into displacement of dynamic glass transition toward higher temperature ranges as a consequence of the immobilization of the elastomeric chains produced by matrix–fiber bonding. There exists a direct correlation between the number of bonds and the observed thermal shift.

On applying the WLF equation to these materials, the respective master curves are obtained, which permit assessment of the dynamic properties in conditions that otherwise cannot be implemented by means of the presently available experimental methods. At very high frequencies the properties are exclusively dependent on the polymeric matrix.

The dynamic properties show anisotropy vis à vis the direction of fiber orientation.

Short fiber-reinforced materials develop a similar behavior for any type of elastomeric matrix used, detected differences being negligible.

REFERENCES

1. L. Ibarra, C. Chamorro, and M. C. Tabernero, *Polym. Composites*, **8**(3), 198 (1988).
2. L. Ibarra, C. Chamorro, and M. C. Tabernero, *Angew. Makromol. Chemie*, **160**, 29 (1988).
3. L. Ibarra and C. Chamorro, *Rev. Plast. Mod.*, **55**(381), 391 (1988).

4. L. Ibarra and C. Chamorro, *Rev. Plast. Mod.*, **54**(373), 89 (1987).
5. L. Ibarra and C. Chamorro, *Polym. Composites*, **10**(4), 256 (1989).
6. L. Ibarra and C. Chamorro, *Rev. Plast. Mod.*, **54**(376), 533 (1987).
7. L. Ibarra and C. Chamorro, *J. Appl. Polym. Sci.*, **37**, 1197 (1989).
8. A. P. Foldi, *Rubber Chem. Technol.*, **49**, 379 (1976).
9. A. Y. Coran, K. Boustany, and P. Hamed, *J. Appl. Polym. Sci.*, **15**, 2471 (1971).
10. P. J. Flory and J. Rehner, *J. Chem. Phys.*, **11**, 512 (1943).
11. A. G. Shvarts, *Rubber Chem. Technol.*, **31**, 691 (1958).
12. T. Noguchi, M. Ashida, and S. Masimo, *Nippon Gomu Kyokaishi*, **57**(3), 171 (1984).
13. P. K. Freakley and A. R. Payne, *Theory and Practice of Engineering with Rubber*, Applied Science Publishers, London, 1978.
14. A. R. Payne and R. E. Whittaker, *Rubber Chem. Technol.*, **44**, 440 (1971).
15. M. Ashida, T. Noguchi, and S. Mashimo, *J. Appl. Polym. Sci.*, **29**, 661 (1984).
16. M. Ashida, T. Noguchi, and S. Mashimo, *J. Appl. Polym. Sci.*, **30**, 1011 (1985).
17. J. D. Ferry, *Viscoelastic Properties of Polymers*, 3rd. ed, Wiley, New York, 1980, Chap. 11.
18. F. R. Eirich, *Science and Technology of Rubber*, Academic Press, New York, 1978, Chap. 15.

Received September 4, 1989
Accepted January 14, 1991